Geophysical Research Letters

RESEARCH LETTER
10.1029/2018GL077996

Key Points:
- Chemical segregation of forsterite does not occur on the microsecond timescales
- Kinetic effects determine the phases present on the forsterite Hugoniot up to 73 GPa

Supporting Information:
- Supporting Information S1

Correspondence to:
M. Newman,
matthew.g.newman@gmail.com

Citation:
Newman, M. G., Kraus, R. G., Akin, M. C., Bernier, J. V., Dillman, A. M., Homel, M. A., et al. (2018). In situ observations of phase changes in shock compressed forsterite. *Geophysical Research Letters*, *45*, 8129–8135. https://doi.org/10.1029/2018GL077996

Received 19 MAR 2018
Accepted 5 JUL 2018
Accepted article online 11 JUL 2018
Published online 17 AUG 2018

In Situ Observations of Phase Changes in Shock Compressed Forsterite

M. G. Newman[1], R. G. Kraus[2], M. C. Akin[2], J. V. Bernier[2], A. M. Dillman[3], M. A. Homel[2], S. Lee[4], J. Lind[2], J. L. Mosenfelder[3], D. C. Pagan[5], N. W. Sinclair[6], and P. D. Asimow[1]

[1]California Institute of Technology, Pasadena, CA, USA, [2]Lawrence Livermore National Laboratory, Livermore, CA, USA, [3]Department of Earth Sciences, University of Minnesota, Minneapolis, MN, USA, [4]High Pressure Science and Engineering Center, University of Nevada, Las Vegas, Las Vegas, NV, USA, [5]Cornell High Energy Synchrotron Source, Ithaca, NY, USA, [6]Dynamic Compression Sector, Institute for Shock Physics, Argonne National Laboratory, Washington State University, Pullman, WA, USA

Abstract Shockwave data on mineral-forming compounds such as Mg_2SiO_4 are essential for understanding the interiors of Earth and other planets, but correct interpretation of these data depends on knowing the phase assemblage being probed at high pressure. Hence, direct observations of the phase or phases making up the measured states along the forsterite Hugoniot are essential to assess whether kinetic factors inhibit the achievement of the expected equilibrium, phase-separated assemblage. Previous shock recovery experiments on forsterite, which has orthorhombic space group Pbnm, show discrepant results as to whether forsterite undergoes segregation into its equilibrium phase assemblage of compositionally distinct structures upon shock compression. Here we present the results of plate impact experiments on polycrystalline forsterite conducted at the Dynamic Compression Sector of the Advanced Photon Source. In situ X-ray diffraction measurements were used to probe the crystal structure(s) in the shock state and to investigate potential decomposition into periclase and bridgmanite. In contrast to previous interpretations of the forsterite shock Hugoniot, we find that forsterite does not decompose but instead reaches the forsterite III structure, which is a metastable structure of Mg_2SiO_4 with orthorhombic space group $Cmc2_1$.

1. Introduction

Knowledge of the equation of state and phase diagram of the MgO-$MgSiO_3$ thermodynamic system is important for modeling the interior structure and dynamics of the Earth's mantle (Asimow, 2017; Fei et al., 2004). Mg_2SiO_4 forsterite has been studied extensively by the high pressure community over a wide range of thermodynamic conditions to understand partial melting and potential chemical stratification of the mantle (Adjaoud et al., 2011; de Koker et al., 2008). Figure 1 shows that at the pressures relevant to the Earth's lower mantle, there is no stable compound with composition Mg_2SiO_4. Therefore, achieving an equilibrium state from an initially homogenous forsterite crystal requires decomposition into at least two compounds. This chemical segregation creates heterogeneous domains from the originally homogeneous material.

Chemical segregation in magnesium silicates is well established in heated static high pressure experiments and further supported by first-principles calculations. Detailed equilibrium experiments in heated multianvil presses show chemical segregation in Mg_2SiO_4 at pressures above 23 GPa (Presnall et al., 1998). First-principles molecular dynamics simulations support chemical segregation of forsterite into a subsolidus phase assemblage of periclase and bridgmanite (de Koker et al., 2013). However, under isothermal compression at 300 K, a series of compounds with Mg_2SiO_4 composition have been shown to remain metastable to 90 GPa, well into the region where chemical segregation to the equilibrium phase assemblage of periclase and bridgmanite is expected to occur (Finkelstein et al., 2014), suggesting that kinetic effects severely inhibit the decomposition process at low temperatures.

As a single component, the bridgmanite structure is stable to 125 GPa, where a phase change to a post-perovskite phase with a $CaIrO_3$ structure has been observed experimentally and confirmed through first-principles calculations (Murakami et al., 2004; Oganov & Ono, 2004). Similarly, the periclase structure

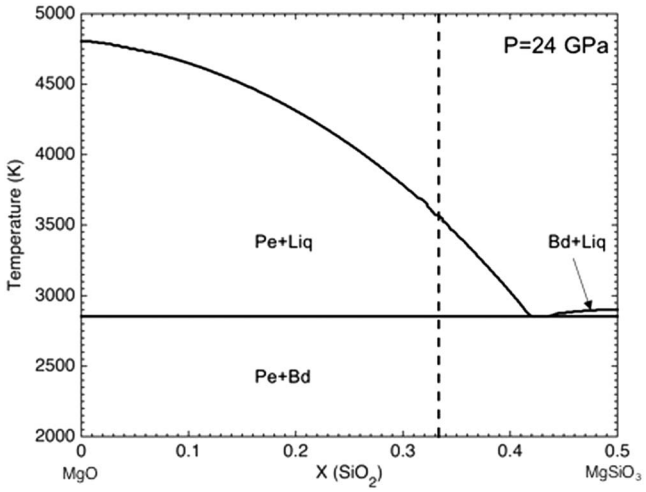

Figure 1. This equilibrium phase diagram of the MgO-$MgSiO_3$ system at 24 GPa shows that there are no thermodynamically stable single component crystal structures of forsterite composition (represented by a vertical dashed line; de Koker et al., 2013). At the pressures and temperatures relevant to this study, forsterite will decompose to bridgmanite (Bd) and periclase (Pe) at equilibrium.

remains stable to 600 GPa, where a phase change from the B1 structure to the B2 structure has been observed experimentally (Coppari et al., 2013). Depending on shock temperature, a number of decomposition paths involving a stable or metastable liquid coexisting with one or more solid phases are also possible.

Uniaxial plate impact experiments provide a platform to measure the high-pressure and high-temperature equation of state of geophysically important materials, where for Earth's lower mantle, the relevant pressure-temperature conditions are bounded below 136 GPa and 3600 K (Nomura et al., 2014). Previous experiments have delineated several phase regions on the forsterite Hugoniot below 136 GPa on the basis of density variations, sound speed measurements, and shock temperature measurements (Brown et al., 1988; Lyzenga & Ahrens, 1980; Mosenfelder et al., 2007). However, no in situ observations of the phase or phases behind the shock front have been made. Therefore, the phase(s) that are attained upon shock compression (metastable or equilibrium) remain undetermined. This issue is particularly pertinent for forsterite, where long timescales of chemical separation limited by ionic diffusion in the solid phase may prevent observation of the equilibrium phase assemblage. To nucleate nanometer size grains, the smallest grains that may reasonably be called stable (Hawreliak et al., 2008; Gleason et al., 2015), on the characteristic microsecond timescale of plate impact experiments requires an ionic diffusivity of 1 $nm^2/\mu s$. This ionic diffusivity is roughly 5 orders of magnitude larger than expected for bulk solid forsterite (Fei, 2013).

Shock recovery experiments, which look for signatures of the shock state in samples recovered to ambient conditions, show disparate results. Samples shocked to 78 GPa and recovered at ambient conditions by Syono, Goto, Takei, et al. (1981) suggest that the nature of the so-called "Mixed Phase" Hugoniot region between 50 and 120 GPa is incomplete transformation to the equilibrium periclase and bridgmanite phase assemblage. Their results are supported by transmission electron microscopy observations of periclase and $MgSiO_3$ glass in the shock recovered samples. In contrast, recovery of samples shocked to pressures up to 75 GPa by Jeanloz (1980) shows no evidence of chemical segregation of forsterite.

Recovery experiments are inherently limited by the assumption that signatures of the shock state are observable at ambient conditions and separable from phenomena, which may occur upon release from the shock state. In situ measurements are necessary to circumvent these limitations. In this paper, we present in situ powder X-ray diffraction observations of the crystal structure of forsterite samples shocked to 44(3) and 73(5) GPa. Our results demonstrate that chemical segregation of forsterite does not occur on dynamic experimental timescales but that nonequilibrium states persist to 73(5) GPa on the forsterite Hugoniot, where the shock temperature is predicted to be ~2500 K (Lyzenga & Ahrens, 1980).

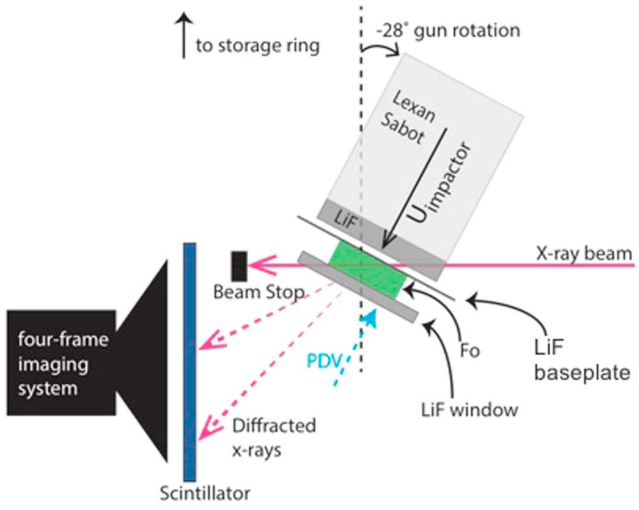

Figure 2. The beam configuration for in situ X-ray diffraction measurements is shown in this schematic drawing. The cylindrical axis of the sample is 28° with respect to the beam direction so that the beam path does not probe laterally released states. The path of the beam penetrates the Lexan sabot, LiF impactor, LiF baseplate, forsterite sample, and LiF window. The driver and window materials are chosen to minimize X-ray attenuation. Diffracted X-rays are collected every 153.4 ns on an LSO scintillator coupled to a four frame imaging system (Luo et al., 2012).

2. Materials and Methods

2.1. Sample Synthesis

Forsterite samples were prepared from high-purity, synthetic forsterite powder with average initial particle size <1μm (Koizumi et al., 2010). The powder was uniaxially pressed into cylindrical dies, removed from the dies, and isostatically cold-pressed at >100 MPa. These cylinders were then vacuum sintered for 5 hr at 1673 K. CT measurements indicated that the resulting forsterite polycrystalline rod, 8 mm in diameter, was free from significant voids and defects. The forsterite rod was cut into five discs of approximately 2-mm thickness and polished flat. The measurements of the ambient forsterite samples are discussed in greater detail in the supporting information.

2.2. Experimental Geometry

The experimental setup used to collect in situ X-ray diffraction from shocked forsterite is shown in Figure 2. The nominal target assembly consisted of a 2-mm-thick forsterite sample sandwiched between a 100-μm-thick lithium fluoride (LiF) baseplate and a 1-mm LiF window. The downrange face of the forsterite sample is coated with 150 nm Al to improve interface reflectivity for velocimetry measurements. The LiF window is used because it is well impedance matched to forsterite and therefore generates a weak release from the shock state. This is important so that the density difference between the shocked and released state is minimized, for a shock state of 73 GPa the release density is only ∼3% less than in the shock state, which enables the X-rays to probe after the shock reaches the LiF window and still obtain a clear diffraction pattern from the high-pressure phase assemblage.

The targets were impacted by a 4-mm-thick LiF single crystal flyer plate mounted in a Lexan Sabot. The low-Z nature of the LiF and Lexan reduce X-ray attenuation, and the single crystal LiF diffraction signature is easy to separate from the polycrystalline forsterite diffraction signal. The sabot was launched by the two-stage light gas gun (12.5-mm bore diameter) at the Dynamic Compression Sector of the Advanced Photon Source, Argonne National Laboratory (DCS), which is capable of generating projectile velocities up to ∼5.7 km/s.

A 23 ± 0.1 keV X-ray pulse of ∼100 ps duration and 0.4-keV FWHM is provided every 153.4 ns by the APS. Diffracted photons are detected on a lutetium oxyorthosilicate (LSO) scintillator coupled to four PIMAX cameras capable of recording four frames per shot (Luo et al., 2012). The axis of the gun was rotated about a vertical axis by 28° relative to the normal of the X-ray beam, such that the path of the beam penetrates the target assembly at 62° to surface normal. The beam is positioned such that laterally released states in the forsterite are not probed by the X-ray pulse.

Table 1
Relative Mass Fraction of the Sample Conditions at X-ray Probe Time

Shot	X-ray time r.b.o. (ns)	Ambient Fo fraction	Shocked Fo fraction	Released Fo fraction
084[a]	−103.6	0.64	0.36	0
084[b]	49.8	0	0.77	0.23
085[a]	−128.9	0.45	0.55	0
085[b]	24.5	0	0.54	0.46

[a]First X-ray pulse. [b]Second X-ray pulse.

Prior to each experiment, polycrystalline Si was placed in the DCS target chamber to calibrate the detector. The Si calibration is used to transform the diffraction data from raw spatial coordinates into the azimuthal and polar diffraction angles, ϕ versus 2θ, where polycrystalline diffraction data project onto lines of constant 2θ. Contour images of the diffraction pattern are integrated with respect to ϕ to produce diffraction patterns (intensity as a function of 2θ).

For diffraction images of the forsterite sample, the calibration is corrected to account for the change in apparent sample-to-detector distance caused by the forsterite thickness. Intense diffraction peaks associated with single-crystal LiF are masked out of the contour image so that they are not integrated into the forsterite diffraction pattern. Comparing the observed ambient forsterite peak positions to theoretical values implies uncertainties in 2θ are ~1%. The calibration for driven forsterite samples is corrected to account for movement of the sample center of mass along the gun axis using the known particle velocity (see discussion of how we calculated particle velocity below) in the shock state. Example calibrated diffraction images for shocked forsterite dewarped into $2\theta - \phi$ space are shown in the supporting information.

Each X-ray pulse is timed relative to shock breakout into the LiF window using an oscilloscope with 50 ps resolution. Using the wave speeds obtained from the Hugoniot relations, we determine the fraction of the shocked, partially released, and unshocked materials, as well as the thermodynamic state of the material (Brown et al., 1988; Duffy & Ahrens, 1992). In both shots, the first frame was observed prior to breakout into the LiF so that a portion of the sample was shocked and the remainder unshocked. The second frame was observed after breakout into the LiF, so that a portion of the sample was shocked and the remainder partially released into LiF. The sample states and pressures probed during the two X-ray pulses are tabulated in Table 1.

Photon Doppler Velocimetry (PDV) was used to monitor the particle velocity, u_p, at the interface between the forsterite sample and LiF window (Strand et al., 2006). The apparent LiF u_p was converted to the true interface velocity using the measured index of refraction for LiF (Rigg et al., 2014). The pressure in the shock state was determined through the standard impedance matching technique using the known Hugoniots of forsterite and LiF (Jackson & Ahrens, 1979; Marsh, 1980; Mosenfelder et al., 2007; Rigg et al., 2014; Syono et al., 1981; Watt & Ahrens, 1983). The release pressure was determined through impedance matching to the reflected forsterite Hugoniot. The pressure states achieved in each experiment are tabulated in Table 2.

3. Results

Full density polycrystalline forsterite was shock compressed to pressures of 44(3) and 73(5) GPa. At 44(3) GPa, we recorded two diffraction images prior to release to ambient pressure, which showed diffraction peaks consistent with forsterite compressed to the Hugoniot density. The processed diffraction image for frame 2 is shown as the middle trace in Figure 3. The peak not identified as compressed forsterite is indexed as diffraction from the (131) plane of the forsterite III structure. The density of the forsterite III structure inferred from the diffraction peak is roughly 10% more dense than the forsterite structure, consistent with previous observations of the equation of state of forsterite and forsterite III (Finkelstein et al., 2014). Matching the

Table 2
Shock and Release Pressure/Density States

Shot	P_{Shock} (GPa)	ρ_{Shock} (g/cm^3)	$P_{Release}$ (GPa)	$\rho_{Release}$ (g/cm^3)
084	44.3(3.0)	4.05(5)	38.2(3.0)	3.96(6)
085	73.4(5.0)	4.57(8)	66.1(5.0)	4.46(9)

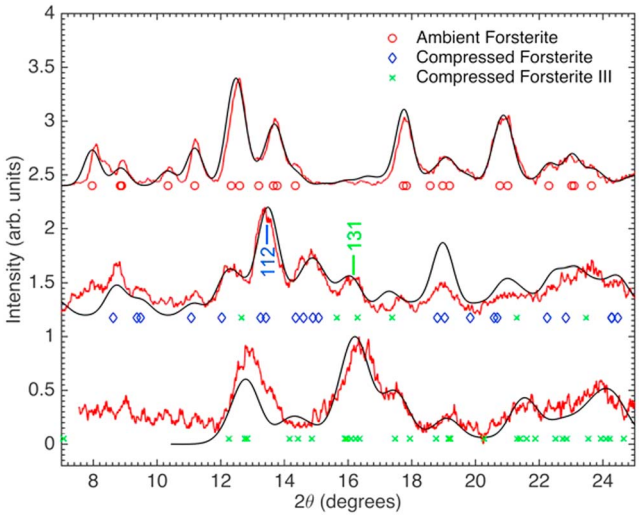

Figure 3. Processed diffraction patterns for ambient forsterite (top), forsterite shocked to 44.3 GPa (middle), and forsterite shocked to 73.4 GPa (bottom). The observed data (red) are compared to theoretical diffraction patterns for the predicted forsterite and forsterite III structures (black).The theoretical diffraction patterns were calculated using Crystal Diffract 6.5, an interactive powder diffraction software.

relative intensity of the (112) forsterite peak and (131) forsterite III peak would suggest a mixture of three parts forsterite to one part forsterite III. Therefore, the error we make by using the Hugoniot density to index the forsterite diffraction peaks is small (on the order of 2%) since the mixture is composed mostly of forsterite. The crystallographic relationship between forsterite and forsterite III is discussed in depth in the work of (Finkelstein et al., 2014).

Upon shock compression to 73(5) GPa, we observe diffraction peak positions consistent with complete transformation to the forsterite III structure, which suggests that the nature of the mixed phase region corresponds to a diffusion free phase transition to forsterite III. The lower trace in Figure 3 shows the processed diffraction data for frame 2, where all of the observed diffraction peaks can be explained by the forsterite III structure.

In the above analysis, we fit lattice parameters to the observed diffraction peaks using the Hugoniot density as an initial guess for the forsterite structures, which was sufficient to assign the crystal structure. Once the

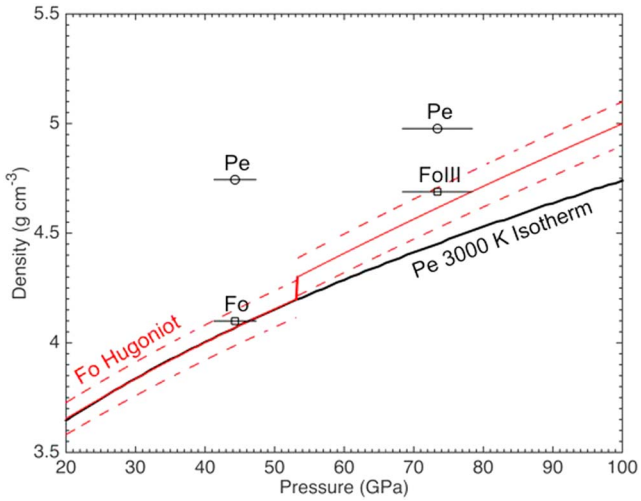

Figure 4. The density of periclase, forsterite, and forsterite III are compared to the expected values based upon the previously measured forsterite Hugoniot and the 3000 K periclase isotherm calculated from equations of state (Mosenfelder et al., 2007; Tange et al., 2009; Wu et al., 2008). The density required to fit the periclase structure is well outside the uncertainty in the periclase isotherm while the forsterite structures are in good agreement with the Hugoniot density.

structures were assigned, the lattice parameters were further refined by minimizing the difference using gradient descent between the observed and theoretical d-spacing for the forsterite and forsterite III structures. The resultant best fit to the data is plotted in Figures S5 and S6. Similarly, the periclase 3000 K isotherm was used as an initial guess for periclase and further refined by minimizing the difference between the observed diffraction and theoretical diffraction from the periclase structure. The 3000-K isotherm was chosen as that represents a reasonable estimate of the temperature on the forsterite Hugoniot at these pressures based upon available data (De Koker & Stixrude, 2009; Luo et al., 2004).

As illustrated in Figure 4, the ambient forsterite structure fit matched the forsterite Hugoniot density within 1% for shot 084, the forsterite III fit matched the forsterite Hugoniot density within 3% for shot 085, and the periclase structure was in poor agreement with the periclase equation of state in both shots (~20% difference in density). This suggests periclase is not present on the forsterite Hugoniot at pressures up to 73(5) GPa.

4. Discussion and Conclusions

Our results show that the previously described "low pressure" Hugoniot regime corresponds to compression of the forsterite lattice and that the nature of the density collapse at 50 GPa is a deformational phase change to the metastable forsterite III structure (Syono, Goto, Sato, et al., 1981). We do not observe the equilibrium phase assemblage of periclase and bridgmanite in the diffraction pattern, consistent with the shock recovery results of Jeanloz (1980), and in disagreement with the recovery experiments of Syono, Goto, Takei, et al. (1981). This suggests either that the MgO observed in recovered products by Syono crystallized after the initial shock state or that other details of the recovery experiment geometry created conditions different from those on the principal Hugoniot.

This data set confirms that significant crystallization of periclase is not observed at the microsecond timescales of the experiment, which bounds the chemical diffusivities in forsterite below 1 $nm^2/\mu s$ at the elevated pressures and temperatures probed in these experiments.

This work provides the first in situ observation of forsterite under uniaxial plate impact conditions. We found that solid state decomposition into the equilibrium phase assemblage (periclase and bridgmanite) is not observed under the kinetic constraints imposed by the timescale of the plate impact experiment, but rather the metastable forsterite III structure persists at the elevated Hugoniot pressures and temperatures. The forsterite and forsterite III structures that we observed are in good agreement with the structures observed at ambient temperature in diamond anvil cells (Finkelstein et al., 2014). Absence of periclase suggests that nucleation from the bulk or localized melt regions does not occur in the material processed by the shock and that diffusion along grain boundaries in forsterite at these conditions is less than previously theorized based on Arrhenius extrapolations from data at lower pressure (Fei, 2013). Future work observing the crystal structure or structures of forsterite in situ at higher pressure would be valuable to determine the nature of the density change along the Hugoniot observed at 120 GPa. The results of this paper illustrate that kinetics, and not equilibrium states, dictate the observed equation of state and material properties on microsecond timescales for multicomponent systems that may phase segregate.

Acknowledgments
This work was performed under the auspices of the U.S. Department of Energy by Lawrence Livermore National Laboratory under Contract DE-AC52-07NA27344. M. G. N., M. C. A., and R. G. K. acknowledge support under grant number 15-ERD-012. M. C. A., J. V. B., D. C. P., J. L., and M. A. H. acknowledge support under LLNL LDRD 16-ERD-010. Portions of this work were performed at GeoSoilEnviroCARS (The University of Chicago, Sector 13), Advanced Photon Source (APS), Argonne National Laboratory. GeoSoilEnviroCARS is supported by the National Science Foundation — Earth Sciences (EAR-1634415) and Department of Energy-GeoSciences (DE-FG02-94ER14466). This publication is based upon work performed at the Dynamic Compression Sector, which is operated by Washington State University under the U.S. Department of Energy (DOE)/National Nuclear Security Administration award DE-NA0002442. This research used resources of the Advanced Photon Source, a U.S. Department of Energy (DOE) Office of Science User Facility operated for the DOE Office of Science by Argonne National Laboratory under contract DE-AC02-06CH11357. J. L. M. acknowledges support from NSF EAR1161023. The data used to generate this report are stored in the Caltech authors repository and can be accessed at http://resolver.caltech.edu/CaltechAUTHORS:20180520-171542198.

References

Adjaoud, O., Steinle-Neumann, G., & Jahn, S. (2011). Transport properties of Mg_2SiO_4 liquid at high pressure: Physical state of a magma ocean. *Earth and Planetary Science Letters*, *312*(3), 463–470.

Asimow, P. D. (2017). A measure of mantle melting. *Science*, *355*(6328), 908–909.

Brown, J. M., Furnish, M. D., & Boness, D. A. (1988). Sound velocities for San Carlos Olivine. In S. C. Schmidt & N. C. Holmes (Eds.), *Shock waves in condensed matter 1987, Proceedings of the Fifth American Physical Society Topical Conference on Shock Waves in Condensed Matter, held in Monterey California, July 20-23, 1987* (pp. 119–122). Amsterdam: North Holland Physics Publishing. ISBN 0 444 87097 0.

Coppari, F., Smith, R., Eggert, J., Wang, J., Rygg, J., Lazicki, A., et al. (2013). Experimental evidence for a phase transition in magnesium oxide at exoplanet pressures. *Nature Geoscience*, *6*(11), 926–929.

de Koker, N., Karki, B. B., & Stixrude, L. (2013). Thermodynamics of the $MgO–SiO_2$ liquid system in Earth's lowermost mantle from first principles. *Earth and Planetary Science Letters*, *361*, 58–63.

De Koker, N., & Stixrude, L. (2009). Self-consistent thermodynamic description of silicate liquids, with application to shock melting of MgO periclase and $MgSiO_3$ perovskite. *Geophysical Journal International*, *178*(1), 162–179.

de Koker, N. P., Stixrude, L., & Karki, B. B. (2008). Thermodynamics, structure, dynamics, and freezing of Mg_2SiO_4 liquid at high pressure. *Geochimica et Cosmochimica Acta*, *72*(5), 1427–1441.

Duffy, T. S., & Ahrens, T. J. (1992). Sound velocities at high pressure and temperature and their geophysical implications. *Journal of Geophysical Research*, *97*(B4), 4503–4520.

Fei, H. (2013). Silicon and oxygen self-diffusion in forsterite and implications to upper-mantle rheology (PhD thesis), Department of Bayerisches Geoinstitut, University of Bayreuth.

Fei, Y., Van Orman, J., Li, J., Van Westrenen, W., Sanloup, C., Minarik, W., et al. (2004). Experimentally determined postspinel transformation boundary in Mg_2SiO_4 using MgO as an internal pressure standard and its geophysical implications. *Journal of Geophysical Research*, *109*, B02305. https://doi.org/10:1029/2003JB002562

Finkelstein, G. J., Dera, P. K., Jahn, S., Oganov, A. R., Holl, C. M., Meng, Y., & Duffy, T. S. (2014). Phase transitions and equation of state of forsterite to 90 GPa from single-crystal X-ray diffraction and molecular modeling. *American Mineralogist*, *99*(1), 35–43.

Gleason, A., Bolme, C., Lee, H., Nagler, B., Galtier, E., Milathianaki, D., et al. (2015). Ultrafast visualization of crystallization and grain growth in shock-compressed SiO_2. *Nature Communications*, *6*, 8191.

Hawreliak, J. A., Kalantar, D. H., Stölken, J. S., Remington, B. A., Lorenzana, H. E., & Wark, J. S. (2008). High-pressure nanocrystalline structure of a shock-compressed single crystal of iron. *Physical Review B*, *78*(22), 220101.

Jackson, I., & Ahrens, T. J. (1979). Shock wave compression of single-crystal forsterite. *Journal of Geophysical Research*, *84*(B6), 3039–3048. https://doi.org/10.1029/JB084iB06p03039

Jeanloz, R. (1980). Shock effects in olivine and implications for Hugoniot data. *Journal of Geophysical Research*, *85*(B6), 3163–3176.

Koizumi, S., Hiraga, T., Tachibana, C., Tasaka, M., Miyazaki, T., Kobayashi, T., et al. (2010). Synthesis of highly dense and fine-grained aggregates of mantle composites by vacuum sintering of nano-sized mineral powders. *Physics and Chemistry of Minerals*, *37*(8), 505–518.

Luo, S.-N., Akins, J. A., Ahrens, T. J., & Asimow, P. D. (2004). Shock-compressed $MgSiO_3$ glass, enstatite, olivine, and quartz: Optical emission, temperatures, and melting. *Journal of Geophysical Research*, *109*, B05205. https://doi.org/10.1029/2003JB002860

Luo, S., Jensen, B., Hooks, D., Fezzaa, K., Ramos, K., Yeager, J., et al. (2012). Gas gun shock experiments with single-pulse x-ray phase contrast imaging and diffraction at the advanced photon source. *Review of Scientific Instruments*, *83*(7), 073903.

Lyzenga, G. A., & Ahrens, T. J. (1980). Shock temperature measurements in Mg_2SiO_4 and SiO_2 at high pressures. *Geophysical Research Letters*, *7*(2), 141–144.

Marsh, S. P. (1980). *LASL Shock Hugoniot Data* (Vol. 5). Berkeley, California: University of California Press.

Mosenfelder, J. L., Asimow, P. D., & Ahrens, T. J. (2007). Thermodynamic properties of Mg_2SiO_4 liquid at ultra-high pressures from shock measurements to 200 GPa on forsterite and wadsleyite. *Journal of Geophysical Research*, *112*, B06208. https://doi.org/10.1029/2006JB004364

Murakami, M., Hirose, K., Kawamura, K., Sata, N., & Ohishi, Y. (2004). Post-perovskite phase transition in $MgSiO_3$. *Science*, *304*(5672), 855–858.

Nomura, R., Hirose, K., Uesugi, K., Ohishi, Y., Tsuchiyama, A., Miyake, A., & Ueno, Y. (2014). Low core-mantle boundary temperature inferred from the solidus of pyrolite. *Science*, *343*(6170), 522–525.

Oganov, A. R., & Ono, S. (2004). Theoretical and experimental evidence for a post-perovskite phase of $MgSiO_3$ in Earth's D'' layer. *Nature*, *430*(6998), 445–448.

Presnall, D. C., Weng, Y.-H., Milholland, C. S., & Walter, M. J. (1998). Liquidus phase relations in the system MgO–$MgSiO_3$ at pressures up to 25 GPa constraints on crystallization of a molten Hadean mantle. *Physics of the Earth and Planetary Interiors*, *107*(1), 83–95.

Rigg, P., Knudson, M., Scharff, R., & Hixson, R. (2014). Determining the refractive index of shocked [100] lithium fluoride to the limit of transmissibility. *Journal of Applied Physics*, *116*(3), 033,515.

Strand, O. T., Goosman, D., Martinez, C., Whitworth, T., & Kuhlow, W. (2006). Compact system for high-speed velocimetry using heterodyne techniques. *Review of Scientific Instruments*, *77*(8), 083,108.

Syono, Y., Goto, T., Sato, J.-i., & Takei, H. (1981). Shock compression measurements of single-crystal forsterite in the pressure range 15–93 GPa. *Journal of Geophysical Research*, *86*(B7), 6181–6186.

Syono, Y., Goto, T., Takei, H., Tokonami, M., & Nobugai, K. (1981). Association reaction in forsterite under shock compression. *Science*, *214*(4517), 177–179.

Tange, Y., Nishihara, Y., & Tsuchiya, T. (2009). Unified analyses for P-V-T equation of state of MgO: A solution for pressure-scale problems in high P-T experiments. *Journal of Geophysical Research*, *114*, B03208. https://doi.org/10.1029/2008JB005813

Watt, J. P., & Ahrens, T. J. (1983). Shock compression of single-crystal forsterite. *Journal of Geophysical Research*, *88*(B11), 9500–9512.

Wu, Z., Wentzcovitch, R. M., Umemoto, K., Li, B., Hirose, K., & Zheng, J.-C. (2008). Pressure-volume-temperature relations in MgO: An ultrahigh pressure-temperature scale for planetary sciences applications. *Journal of Geophysical Research*, *113*, B06204. https://doi.org/10.1029/2007JB005275